JOURNAL OF NEUROTRAUMA 28:1185–1198 (July 2011)

DOI: 10.1089/neu.2011.1756

# Traumatic Axonal Injury in the Optic Nerve: Evidence for Axonal Swelling, Disconnection, Dieback, and Reorganization

Jiaqiong Wang, Robert J. Hamm, and John T. Povlishock

**Abstract**

Traumatic axonal injury (TAI) is a major feature of traumatic brain injury (TBI) and is associated with much of its morbidity. To date, significant insight has been gained into the initiating pathogenesis of TAI. However, the nature of TAI within the injured brain precludes the consistent evaluation of its specific anterograde and retrograde sequelae. To overcome this limitation, we used the relatively organized optic nerve in a central fluid percussion injury (cFPI) model. To improve the visualization of TAI, we utilized mice expressing yellow fluorescent protein (YFP) in their visual pathways. Through this approach, we consistently generated TAI in the optic nerve and qualitatively and quantitatively evaluated its progression over a 48-h period in YFP axons via confocal microscopy and electron microscopy. In this model, delayed axonal swelling with subsequent disconnection were the norm, together with the fact that once disconnected, both the proximal and distal axonal segments revealed significant dieback, with the proximal swellings showing regression and reorganization, while the distal swellings persisted, although showing signs of impending degeneration. When antibodies targeting the C-terminus of amyloid precursor protein (APP), a routine marker of TAI were employed, they mapped exclusively to the proximal axonal segments without distal targeting, regardless of the survival time. Concomitant with this evolving axonal pathology, focal YFP fluorescence quenching occurred and mapped precisely to immunoreactive loci positive for Texas-Red-conjugated-IgG, indicating that blood–brain barrier disruption and its attendant edema contributed to this phenomenon. This was confirmed through the use of antibodies targeting endogenous YFP, which demonstrated the retention of intact immunoreactive axons despite YFP fluorescence quenching. Collectively, the results of this study within the injured optic nerve provide unprecedented insight into the evolving pathobiology associated with TAI.

**Key words:** anterograde and retrograde axonal change; amyloid precursor protein; axonal dieback; brain edema; traumatic brain injury; YFP mice

## Introduction

Traumatic axonal injury (TAI) is a major feature of human traumatic brain injury (TBI) (Povlishock and Katz 2005), and has been associated with much of its morbidity (Graham et al., 2002). This has recently been reaffirmed by the use of modern imaging tools, including diffusion tensor imaging, which consistently demonstrates the presence of axonal injury across the spectrum of mild to severe TBI (Belanger et al., 2007; Kumar et al., 2010; Wang et al., 2008). In human postmortem studies, as well as in experimental animal investigations, significant insight has been gained into its initiating pathogenesis (Blumbergs et al., 1989; Büki et al., 2000; Christman et al., 1994; Farkas and Povlishock, 2007; Kelley et al., 2006; Maxwell et al., 1997; Pettus and Povlishock, 1996; Povlishock, 1992; Povlishock and Katz, 2005; Saatman et al., 2003, 2009; Sulaiman et al., 2010), and its potential therapeutic management (Büki et al., 2003; Deng-Bryant et al., 2008; Hall et al., 2010; Kilinc et al., 2007; Koizumi and Povlishock, 1998; Marmarou and Povlishock, 2006; Mbye et al., 2009; Maxwell et al., 2005; Oda et al., 2010; Okonkwo et al., 1999; Saatman et al., 2010).

Despite this progress, however, a fully comprehensive appreciation of TAI has been limited by both technical and animal modeling issues that have precluded the possibility of experimentally analyzing the course of a single nerve fiber

Department of Anatomy and Neurobiology, Virginia Commonwealth University Medical Center, Richmond, Virginia.

from its initial injury to its ultimate axotomy. Further, although various antibodies have been widely embraced in both humans and animals to target such evolving axonal pathology, it is unclear if these antibodies, many of which target amyloid precursor proteins (APP; Blumbergs et al., 1995; Hortobagyi et al., 2007; Sherriff et al., 1994a, 1994b; Stone et al., 2000), universally detect axonal change within the proximal disconnected axonal segment versus the more distal, disconnected segment, or both. This issue is of more than academic interest in that these antibodies are routinely used in human forensic analysis (Gleckman et al., 1999; Reichard et al., 2005).

To better follow the proximal and distal progression of traumatically-induced axonal injury, we assessed in the current study the relationship of known biological markers of axonal injury in an animal central fluid percussion injury (cFPI) model that evokes TAI within the optic nerve, whose axons manifest a relatively organized alignment. Further, to better follow the fate of these damaged axonal segments and their relation to known immunocytochemical markers of axonal injury, we utilized transgenic animals expressing yellow fluorescent protein (YFP), a variant of green fluorescent protein (GFP), in the optic nerve. Through the use of qualitative and quantitative imaging approaches examining the YFP-expressing injured axons, we confirm and significantly extend previous data supporting the delayed pathogenesis of TAI. Importantly, we also provide unprecedented insight into this complex pathology, demonstrating post-TBI axonal swelling and disconnection, with proximal and distal axonal dieback accompanied by the regression and reorganization of the proximal axonal swellings, and the degeneration and delayed clearance of the distal swellings.

## Methods

To visualize axonal damage within the optic nerve, we utilized C57/BL6 wild-type mice and Thy1-YFP-16 transgenic mice which express YFP under the promoter Thy1 within over 80% of the optic nerve fibers (Feng et al., 2000). We posited that within such a YFP-positive fiber population, any potential axonal change induced by the traumatic event could be easily and consistently visualized via routine fluorescence and/or confocal microscopy.

### *Breeding and genotyping of YFP-16 transgenic mice*

The Thy1-YFP-16 transgenic mice [B6.Cg-Tg(Thy1-YFP)16Jrs/J, stock number 003709] were obtained from the Jackson Laboratory (Bar Harbor, ME) and maintained as heterozygotes. Inheritance of the YFP gene was identified from an ear punch taken at weaning (approximately postnatal day 21). The ear tissue was mounted onto a glass slide and examined using a FITC filter on an Olympus DP71 digital camera (Olympus, Center Valley, PA), where YFP-positive axons could be easily identified.

### *Surgery and animal model of traumatic brain injury*

All protocols used in this study were approved by the Institutional Animal Care and Use Committee (IACUC) of Virginia Commonwealth University. Adult male C57/BL6 mice and Thy1-YFP-16 transgenic mice (20–25 g) were subjected to central fluid percussion TBI to produce TAI in the optic nerve. The fluid percussion injury model was modified from that previously described in detail by Dixon (1987). Briefly, animals were anesthetized with 4% isoflurane in 100% $O_2$, and maintained via nosecone with 2% isoflurane in 100% $O_2$ during surgery, with the body temperature controlled at 37°C via a feedback-controlled heating pad (Harvard Apparatus, Holliston, MA). A midline 3.0-mm circular craniotomy was made over the sagittal suture halfway between the bregma and the lambda, taking care not to damage the underlying dura. A Luer-Loc syringe hub was cut away from a 20 gauge needle and affixed to the craniotomy site. Dental acrylic was applied around the hub to enhance stability. As the dental acrylic dried and the injury hub became stable, saline was applied to blunt any exothermic reaction from the cured acrylic. The skin was then sutured over the hub, with lidocaine and bacitracin ointment applied to the wound. The animal was allowed to recover for 1 h in a warmed cage prior to injury. Before the induction of injury, each animal was again anesthetized for 4 min (100% $O_2$ and 4% isoflurane). The craniotomy site was exposed and the injury hub was connected to the fluid percussion device. The animal was then injured at a magnitude of $1.40 \pm 0.05$ atmospheres. The pressure pulse was measured by a storage oscilloscope (Tektronix 5111; Tektronix, Beaverton, OR). Injury preparation and induction were completed prior to the animal's recovery from anesthesia. The hub and dental acrylic were then removed, and the incision was rapidly sutured. The duration of transient unconsciousness was determined by measuring the time it took for the animal to recover the following reflexes: toe pinch, tail pinch, corneal blink, pinna, and righting reflex. After recovery of the righting reflex, the animals were placed in an incubator with a heating pad to maintain normothermia and monitored during recovery. For animals receiving sham injury, all of the above steps were followed with the exclusion of the injury pulse. All injured animals had righting reflex recovery times of 4–5 min, compared with less than 2 min for sham-injured animals, indicating injuries of comparable severity. The animals were allowed to survive 5 min, 15 min, 1 h, 3 h, 12 h, 24 h, and 48 h following injury.

### *Optic nerve preparation*

At the appropriate survival times, Thy1-YFP-16 transgenic mice and wild-type mice were euthanized via an intraperitoneal overdose of sodium pentobarbital, and then transcardially perfused with 100 mL heparinized normal saline, followed by 200 mL 4% paraformaldehyde in Millonig's buffer. After overnight incubation in the perfusion fixative solution, the optic nerve, chiasm, and optic tract, together with the brain were removed from the skull for routine fluorescence and confocal analysis. The optic nerves were blocked to include the entire optic nerve, the chiasm, the initial part of the optic tract, and related brain tissue, and post-fixed in the same solution overnight. Following post-fixation, this optic nerve block was cryoprotected and then cut longitudinally into 10-$\mu$m sections with a cryotome (Shandon Scientific Ltd., Cheshire, U.K.). Serial sections revealing the entire length of the optic nerve (from the globe to the chiasm) were then collected in a serial order. All sections were collected beginning at a randomly generated starting point in Millonig's buffer in 24-well culture plates (Falcon, Newark, DE). Beginning at a random starting point, every fourth serial section was then

prepared for the visualization of the YFP. These sections were directly mounted on glass slides with ProLong® Gold antifade reagent (Invitrogen, Carlsbad, CA), and cover-slipped for image capture with a Leica TCS-SP2 AOBS confocal microscope (Wetzlar, Germany) under the same setting. The adjacent serial sections were used for immunohistochemical staining via antibodies targeting APP. Next, the adjacent serial sections were prepared for the evaluation of potential blood–brain barrier (BBB) disruption via antibodies targeting IgG. Lastly, the subsequent adjacent serial sections were used for determining axonal integrity via antibodies targeting the endogenous YFP (see below).

### *Immunohistochemistry*

To study the relationship between the YFP-linked axonal change and an established biological marker of axonal pathology, antibodies targeting APP were used. YFP fluorescent optic nerve sections were microwaved for antigen retrieval (Stone et al., 1999, 2000), incubated with the primary antibody rabbit anti-C-terminus APP (1:1000; Zymed, San Francisco, CA), washed, and then incubated in the secondary antibody Alexa 594-conjugated goat anti-rabbit IgG (1:200, Vector Laboratories, Burlingame, CA). Then the sections were washed and mounted for analysis via confocal microscopy.

Additionally, to determine if these axonal changes were related to BBB disruption, with the formation of edema and its potential quenching of the YFP fluorescence, we probed the adjacent optic nerve sections with the antibody Texas-Red-conjugated goat anti-mouse IgG (1:200; Invitrogen), targeting mouse serum proteins, and mapping any potential changes in BBB status with any related loss of YFP fluorescence.

Lastly, to determine the potential for axonal preservation despite the loss of YFP fluorescence due to YFP fluorescence quenching, we reacted the subsequent adjacent segments with antibodies targeting the endogenous YFP. Briefly, after antigen retrieval in a microwave, YFP-expressing optic nerve sections were incubated with a primary antibody rabbit anti-GFP (1:8000; Chemicon, Temecula, CA). This was done because YFP and GFP share the same structure (Shagin et al., 2004). Thus, antibodies to GFP also recognize the YFP antigen (Sprecher and Desplan, 2008). Next, the sections were washed, followed by incubation in the secondary antibody Alexa 594-conjugated goat anti-rabbit IgG (1:500; Vector Laboratories) for confocal microscopic analysis. In these immunocytochemical/confocal studies 5 injured mice were evaluated per time point, with the evaluation of 1 sham injured control per time point.

### *Electron microscopy*

For electron microscopic (EM) analysis, additional mice were employed to include 1 injured wild-type mouse, 1 injured YFP-expressing mouse, and their appropriate sham injured controls per time point. In these animals, two different perfusion protocols were employed to achieve: (1) optimal ultrastructure detail, or (2) the optimal visualization of the YFP-positive axons. To achieve optimal ultrastructure detail, wild-type mice were first perfused with 100 mL heparinized normal saline, followed by 200 mL 2% paraformaldehyde and 2.5% glutaraldehyde in Millonig's buffer. For EM analysis of the Thy1-YFP-16 transgenic mice, the animals were first perfused with 100 mL heparinized normal saline, followed by 200 mL 4% paraformaldehyde and 0.2% glutaraldehyde in Millonig's buffer in order to maintain the structure of YFP fluorescent protein and optimize immunoreactivity. Again, the brain and the optic nerves were post-fixed and blocked as described above. For routine EM study the whole optic nerve was osmicated, dehydrated, and flat embedded in epoxy resin (Embed-812; Electron Microscopy Sciences, Hatfield, PA) as detailed below. In contrast, for the YFP-expressing mice, the optic nerve sections were cut longitudinally at 16 $\mu$m with a vibratome (Leica VT1000 S; Leica Microsystems GmbH, Nussloch, Germany), and then prepared for immunocytochemistry using a primary antibody rabbit anti-GFP (1:8000; Chemicon) followed by the secondary antibody, biotinylated goat anti-rabbit IgG (1:1000; Vector). Next, the tissue was incubated in avidin-biotin complex (1:200, Vectastain ABC Standard Elite Kit; Vector Laboratories), and visualized by diaminobenzidene (DAB; Sigma-Aldrich, St. Louis, MO) for subsequent EM analysis.

Briefly, the above-prepared immunoreactive YFP-expressing sections were osmicated in 1% $OsO_4$, dehydrated, embedded in epoxy resins, mounted on plastic slides (Thomas Scientific Co., Swedesboro, NJ) and cover-slipped. After resin curing, the plastic slides were examined via routine light microscopy to identify the injured axonal segments within the optic nerve based on the patterns of distribution seen in the YFP-expressing mice previously evaluated by confocal microscopy. Once identified, these sites were excised, mounted on plastic studs, and thick sectioned to the depth of the immunoreactive sites of interest using an ultramicrotome (Leica Ultracut R; Leica, Wien, Austria). Serial 40-nm sections were cut and mounted onto Formvar-coated single-slotted grids. The grids were then stained with 5% uranyl acetate in 50% methanol for 2 min and 0.5% lead citrate for 1 min, and visualized using a JEM 1230 electron microscope (JEOL Ltd., Tokyo, Japan).

### *Confocal microscopic data analysis*

At the 12-, 24-, and 48-h time points, quantitative analysis of any observed axonal swelling detected by confocal imaging was conducted. The randomly selected YFP optic nerve sections were analyzed via the placement of 12 serial grids (each grid = 200 $\mu$m × 200 $\mu$m) along the optic nerve, six of which were placed proximally and labeled P1–P6 moving from the initial locus of TAI (approximately 1 mm rostral to the chiasm) to the globe, and the other six of which were located distally and labeled D1–D6 moving from the initial locus of TAI to the chiasm. Each 200 $\mu$m × 200 $\mu$m grid was aligned over the center of the optic nerve. For each individual grid, the number of axonal swellings per unit area, the total area of axonal swellings per unit area, and the percentage of the total area of axonal swellings per unit area, as well as the size of axonal swellings per unit area were measured using the Imaging Processing (IP) Lab 3.7 image analysis system (Scanalytics, Inc., Fairfax, VA). Only those swellings over 5 $\mu$m in diameter were analyzed (Gao et al., 2010). Any swellings overlapping either the top, the bottom, or the left line of the grid were included, while those overlapping the right grid line were excluded from analysis. All results were presented as mean ± standard error of the mean (SEM). Each dependent variable was analyzed separately by a split-plot analysis of variance [ANOVA; 3 (Time) × 12 (Location)]. To examine the

specific effect of time for each dependent variable at each of the locations, subsequent one-factor (time) ANOVAs and *post-hoc* Fisher LSD tests were conducted for each grid location. Statistical significance was set at $p < 0.05$ for all tests.

## Results

### *Macroscopic changes in the mouse brain and optic nerve*

Using this model system, which was modified from that previously used in rats (Dixon et al., 1987), we consistently generated microscopic injury in the optic nerve (see below), without overt damage to the brain tissue. As shown in Figure 1A, the injured brain revealed no significant contusion, parenchymal hemorrhage, or overt damage of the optic nerve and/or the globe. Macroscopic brain sectioning again revealed no damage within the brain parenchyma, either in terms of intraparenchymal petechial hemorrhage or blood in the intraventricular space.

### *Qualitative fluorescent microscopic change within the optic nerve following TBI*

Despite the lack of macroscopic damage in this model, axonal damage was evoked in a scattered fashion throughout the brain parenchyma as well as the optic nerve of Thy1-YFP-16 transgenic mice following TBI. While not the focus of the current communication, within the brain parenchyma itself, scattered axonal damage could be identified within both the superficial and deep layers of the neocortex, as well as the dorsolateral thalamus and subcortical white matter. These findings are entirely consistent with those recently reported in the same mouse injury model using a YFP-H mouse (Greer et al., 2011). Importantly, in the current study these axonal changes occurred without any evidence of local petechial hemorrhage and/or any other form of tissue disruption, consistent with a mild TBI. Within the optic nerve, the traumatic axonal injury typically was induced approximately 1 mm proximal to the chiasm. As will be detailed below, within this locus, scattered reactive axonal change could be observed in YFP-expressing axons, while adjacent YFP axons maintained normal structural detail. These findings stood in stark contrast to the sham-injured animals, wherein numerous linear/non-swollen YFP-expressing axonal profiles (Fig. 1B) could be seen spanning the length of the optic nerve, consistent with the initial characterization of the Thy1-YFP-16 transgenic mouse (Feng et al., 2000).

Consistent with previous descriptions of traumatically induced axonal damage, the injured YFP-expressing axons demonstrated a progression of reactive change over time. At 1 h post-TBI, the majority of axons manifested normal morphology, with only scattered axons demonstrating punctuate,

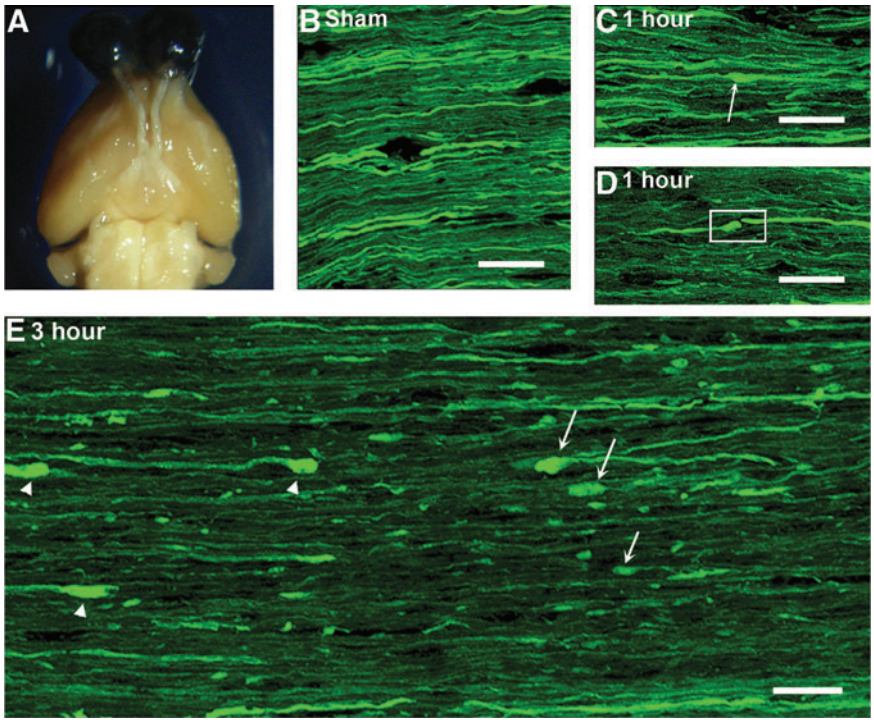


**FIG. 1.** A macroscopic view of the injured brain and the optic nerve together with the microscopic evidence of axonal damage in the optic nerve of Thy1-YFP-16 mice. Note that upon macroscopic examination, no significant contusion, mass lesion, or hemorrhage can be identified within either the brain or the optic nerve following TBI (**A**). Via confocal microscopy, the optic nerve of the sham-injured mice reveals a robust distribution of YFP-positive axons maintaining continuity with no evidence of axonal swelling (**B**). At 1 h post-TBI, the majority of YFP-positive axons manifest normal morphology, with only scattered, punctate axonal swelling (arrow in **C**), and isolated axonal disconnection (box in **D**). At 3 h post-TBI, note the increase in both the number and the size of axonal swellings in both the proximal (arrows in **E**) and distal segments (arrowheads in **E**). Also note that the disconnection of many damaged axons occurs interspersed among adjacent intact fibers. In this image, the chiasm is to the left and the globe lies to the right (scale bars = 20 $\mu$m).

focal YFP-fluorescent axonal swellings (Fig. 1C), as well as some evidence of initial axonal disconnection (Fig. 1D). These scattered punctuate swellings were typically found at only one locus along the axon's length, without any evidence of additional proximal to distal involvement.

By 3 h post-TBI, focal axonal disconnection was now prominent together with a significant increase in the number and the size ($8.32 \pm 0.69\ \mu$m) of the YFP-expressing axonal swellings, which now capped both the proximal and distal disconnected segments. Again, these damaged axons were interspersed among adjacent intact fibers (Fig. 1E). At this time point, those proximal axonal swellings maintaining continuity with the retina (arrow in Fig. 1E) appeared bulbous/spheroidal in shape. The distal axonal swellings on those axons projecting to the chiasm were also spheroidal (arrowhead in Fig. 1E). As now both the proximal and distal swellings were frequently separated, this suggested axonal retraction or dieback, an issue further detailed below.

By 12 h post-TBI, the above described YFP-expressing axonal swellings exhibited further maturation (Fig. 2A), with axonal disconnection now predominating. The proximal axonal swellings had expanded to an area of $28.26 \pm 2.00\ \mu m^2$, and now revealed a more truncated configuration (Fig. 2C and 2E). In contrast, the distal axonal swellings continued to expand ($25.53 \pm 1.38\ \mu m^2$), yet maintained their more rounded/spheroidal shape (Fig. 2B and 2D). From 24 h to 48 h post-TBI, the distal axonal swellings underwent further expansion ($42.78 \pm 5.88\ \mu m^2$ at 24 h post-TBI, and $50.84 \pm 2.48\ \mu m^2$ at 48 h post-TBI), with their distribution shifted more distally toward the chiasm. Similarly, the proximal axonal swellings now redistributed from the initial site of injury to the more proximal segments of the optic nerve approaching the globe. In contrast to the distal segments, however, these proximal truncated segments showed continued evidence of shrinkage and resorption.

While these axonal findings at 12, 24, and 48 h post-TBI were scattered, routine confocal analysis revealed that these reactive axonal changes and dieback were accompanied by an apparent focal loss of fluorescence in the region between the detached proximal and distal axonal segments. At first, this was interpreted to reflect total fiber loss in this now non-fluorescent domain. However, as will be explicated below, this apparent fluorescent fiber loss was not the result of actual fiber dissolution. Rather it was the result of local fluorescence quenching, a sequela of local BBB disruption discussed below.

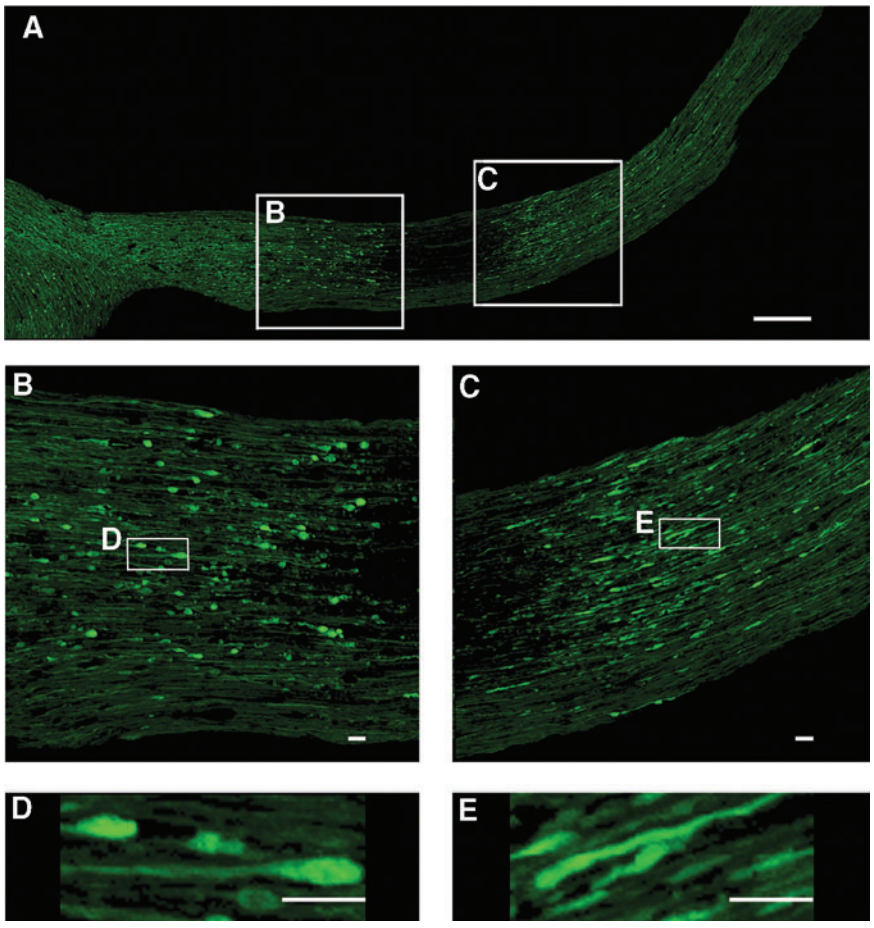


**FIG. 2.** Confocal microscopic evidence of axonal swellings within the optic nerve of Thy1-YFP-16 mice at 12 h post-TBI. Note that the axonal swellings now manifest further maturation (**A**). Additionally note that the distal axonal swellings expand to form spheroids (**B** and **D**), while the proximal axonal swellings now assume a more truncated form (**C** and **E**; scale bar = 200 $\mu$m in **A**, 20 $\mu$m in **B**, **C**, **D**, and **E**).

### *Electron microscopic evaluation of the traumatic axonal damage*

EM analysis confirmed and supplemented the above-described fluorescence analysis. Via EM analysis of the wild-type mice, we observed as early as 5 to 15 min post-TBI, scattered axons located approximately 1 mm rostral to the optic chiasm demonstrating initial axonal swelling, associated with an accumulation of mitochondria (M in Fig. 3). Despite these local reactive changes, adjacent axons remained intact and displayed normal ultrastructural detail, all of which was consistent with previous descriptions of TAI. In these same regions, edematous-like change could also be identified via the expansion of the interstitial space (asterisk in Fig. 3). Additionally, by 1 h post-TBI, there was local dissolution of some damaged axons, consistent with the process of disconnection and separation (arrowhead in Fig. 3).

By 3 h post-TBI, axonal detachment was common in the Thy1-YFP-16 mice, with both the proximal and distal axonal swellings now easily recognized. As observed via confocal microscopy above, both proximal and distal swellings were spheroidal, with obvious separation between the proximal and distal swellings. Although it proved difficult to follow the course of one individual separated axon via electron microscopy, examination of numerous serial sections revealed that the proximal and distal swellings were separated by highly vacuolated and organelle-devoid axonal cylinders, suggesting that they were the residual axonal segments that once joined both the proximal and distal swellings. The proximal swelling appeared reminiscent of previous descriptions of TAI in that the swelling itself contained numerous profiles of smooth endoplasmic reticulum and vesicles which were interspersed with intact mitochondria and multiple vesicular profiles embedded in an electron-lucent axoplasm (Povlishock et al., 1983). This proximal organelle cap typically encompassed a disorganized cytoskeletal core containing misaligned neurofilaments and microtubules. The distal swellings also showed organelle accumulation and a disorganized cytoskeletal core (Fig. 4). However, unlike the proximal segments, these swellings were typically electron dense, and they contained numerous dilated mitochondria with disorganized cristae (M in Fig. 4), all of which appeared consistent with an ongoing degenerative process.

By 24 h post-TBI of the Thy1-YFP-16 mice, the distal swellings enlarged further, once again containing numerous mitochondria with disordered cristae, as well as occasional autophagic vacuoles and lysosomal debris (Fig. 5C and D). In contrast to the distal swellings, the proximal axonal swellings, similarly to those observed via confocal fluorescence microscopy, were now truncated (Fig. 5A and B). Typically, these truncated segments were encompassed by an intact myelin sheath, and contained numerous organelles, all of which appeared intact (Fig. 5B). Specifically, these truncated appendages contained numerous mitochondria, profiles of smooth endoplasmic reticulum and vesicles, as well as cytoskeletal constituents, all of which revealed normal morphological detail. In contrast to the distal swellings, not only did these proximal swellings reveal intact mitochondria, but importantly, these organelles were found in an electron-lucent environment, with no evidence of increased electron density.

### *Quantitative analysis of the progressive axonal swellings and dieback in the proximal and distal segments*

As noted, the quantitative analysis conducted in the current investigation employed confocal microscopy to assess the number of axonal swellings per unit area, the total area of axonal swellings per unit area, the percentage of the total area of axonal swellings per unit area, as well as the size of axonal swellings per unit area. As noted, these measures were examined along the proximal to distal extent of the optic nerve, with a grid analysis (Fig. 6) that moved both proximally and distally from the point of injury initiation.

While examining the total number of axonal swellings within each grid, a plot-plot ANOVA on these data yielded a significant main effect of location ($F_{11,66} = 81.31$, $p < 0.001$), and a Time × Location interaction ($F_{22,66} = 22.44$, $p < 0.001$). Figure 7 displays a line graph (Fig. 7A) and a bar graph (Fig. 7B) of the same data set, along with the results of the Fisher LSD tests that examined significant group differences at each axonal location. In the proximal portion of the optic nerve, the peak number of axonal swellings per unit area revealed significant redistribution from 200 $\mu$m–400 $\mu$m (grid P2) at 12 h post-TBI ($97.44 \pm 7.61$), to 400 $\mu$m–600 $\mu$m (grid P3) at 24 h post-TBI ($53.22 \pm 9.56$), and approaching 600 $\mu$m–800 $\mu$m (grid P4) at 48 h post-TBI ($46.55 \pm 4.05$). These data suggested a dieback of the proximal disconnected axons over time. Similarly, axonal swellings in the distal segment moved in the opposite direction toward the chiasm. Specifically, here the peak number of axonal swellings per unit area moved from 200 $\mu$m–400 $\mu$m (grid D2) at 12 h post-TBI ($87.56 \pm 13.36$), to 400 $\mu$m–600 $\mu$m

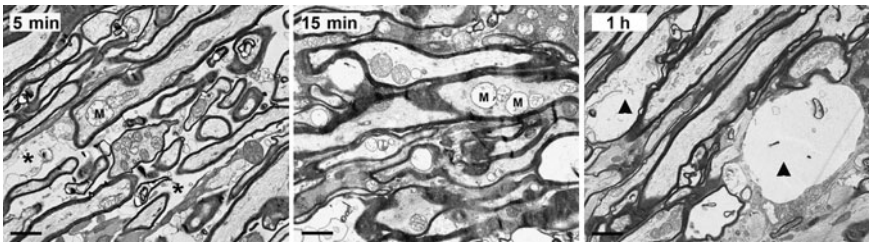


**FIG. 3.** Electron microscopic evidence of the progression of axonal damage in the optic nerve of wild-type mice from 5 min to 1 h post-TBI. Note that at 5 min and 15 min post-TBI the initial axonal swellings are associated with accumulation of mitochondria, some of which are swollen (M). Also note the related expansion of the extracellular space consistent with the presence of edema (asterisk). Lastly, note that at 1 h post-TBI damaged axons reveal local dissolution (arrowhead), consistent with the process of disconnection, which is present in the optic nerve of Thy1-YFP-16 mice (scale bars = 1 $\mu$m).

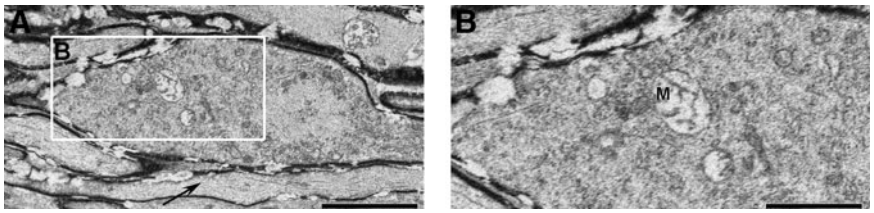


**FIG. 4.** Electron microscopic evidence of axonal swelling in the optic nerve of Thy1-YFP-16 mice at 3 h post-TBI. At this time point the distal axonal swellings display continued maturation, with the accumulation of numerous vesicles and organelles which overlie a disorganized cytoskeletal core (**A**). Note that in the enlarged image (**B**), the dilated mitochondria exhibit disorganized cristae (M). Also note that in contrast to the swollen damaged axon, the adjacent axon remains intact (arrow in **A**; scale bar = 2 $\mu$m in **A**, 1 $\mu$m in **B**).

(grid D3) at 24 h post-TBI (87.11 ± 8.78), and approaching 600 $\mu$m–800 $\mu$m (grid D4) at 48 h post-TBI (103.78 ± 1.73). These quantitative findings confirmed those qualitative impressions of proximal swelling and regression as well as distal expansion and retention, all of which were associated with dieback.

Comparable to the data discussed in terms of the number of axonal swellings, a similar relationship was found in the total area of the axonal swellings per unit area over time along the length of the optic nerve. As shown in Figure 8, a plot-plot ANOVA on these data again revealed a significant main effect of location ($F_{11,66} = 68.85$, $p < 0.001$), and a Time × Location interaction ($F_{22,66} = 19.27$, $p < 0.001$). In the proximal segment, the peak total area of axonal swellings was redistributed from 200 $\mu$m–400 $\mu$m proximal to the lesion (grid P2) at 12 h post-TBI (2203.67 ± 216.93 $\mu m^2$), to 400 $\mu$m–600 $\mu$m proximal to the lesion (grid P3) at 24 h post-TBI (1502.28 ± 42.09 $\mu m^2$), and further to 600 $\mu$m–800 $\mu$m proximal to the lesion (grid P4) at

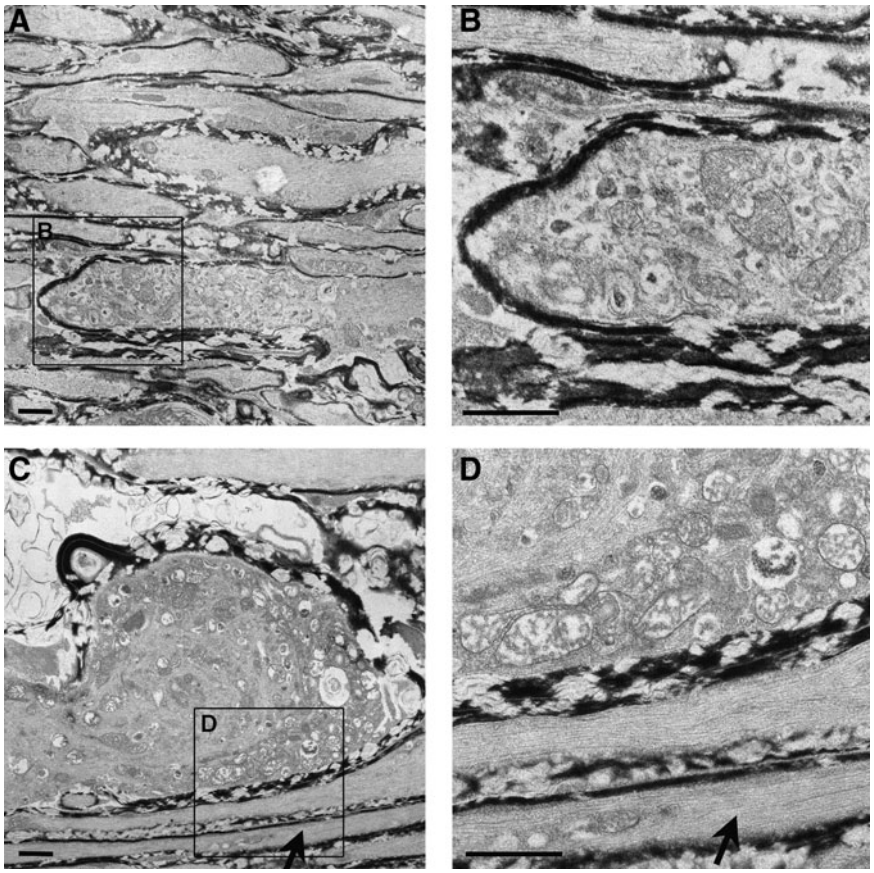


**FIG. 5.** Electron microscopic evidence of progressive axonal swelling in the optic nerve of Thy1-YFP-16 mice at 24 h post-TBI. Now the proximal axonal swelling is more truncated (**A** and **B**), with numerous vesicles and smooth endoplasmic reticulum accumulating in the swollen axonal segment (**B**), while the related mitochondria remain intact (**B**). In contrast, the distal axonal swelling continues to expand and becomes increasingly rounded (**C**). Note the swollen mitochondria with disordered cristae (**D**) accumulating within the swollen bulb (**C** and **D**). Also note the presence of isolated continuous non-axotomized fibers coursing adjacent to the swollen axons at this time point (arrows in **C** and **D**; scale bars = 1 $\mu$m).

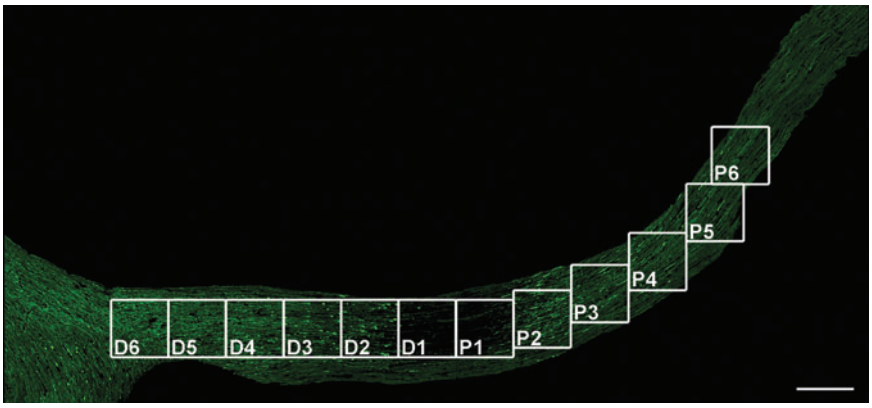


**FIG. 6.** The location of 12 grids along the YFP-expressing optic nerve for quantitative assessment. In this study, each grid encompasses 200 $\mu$m × 200 $\mu$m. From the initial locus of TAI, grids P1 to P6 are placed along the proximal segment approaching the globe, while grids D1 to D6 are located in the distal segment approaching the chiasm (scale bar = 200 $\mu$m).

48 h post-TBI (1006.01 ± 137.07 $\mu m^2$). In the distal segment, the peak total area of axonal swellings migrated from 200 $\mu$m–400 $\mu$m distal to the lesion (grid D2) at 12 h post-TBI (2271.54 ± 451.63 $\mu m^2$), to 400 $\mu$m–600 $\mu$m distal to the lesion (grid D3) at 24 h post-TBI (3689.21 ± 294.12 $\mu m^2$), and further to 600 $\mu$m–800 $\mu$m distal to the lesion (grid D4) at 48 h post-TBI (5267.26 ± 209.76 $\mu m^2$). This again demonstrated progressive axonal dieback in both the proximal and distal directions along the optic nerve post-TBI.

Similarly, the analysis on the percentage of the total area of axonal swellings per unit area revealed a statistically significant relationship comparable to that described above over time along the length of the optic nerve (data not shown). In contrast, the analysis of the size of axonal swellings per unit

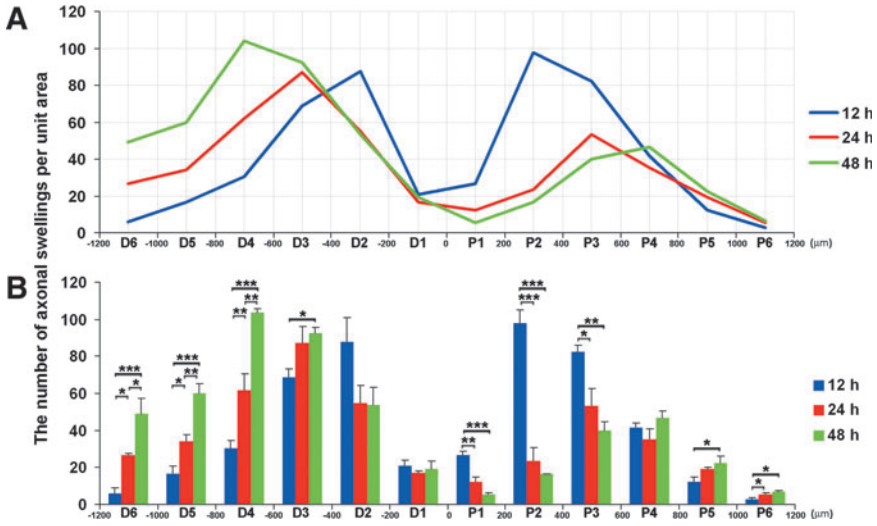


**FIG. 7.** A plot of the number of axonal swellings per unit area and their distribution along the optic nerve over time. In both the line (**A**) and bar (**B**) graph, a significant difference exists between the number of axonal swellings at each time point at the related region ($p < 0.05$). The line graph (**A**) best illustrates the change of axonal swelling distribution along the optic nerve over time (blue = 12 h, red = 24 h, and green = 48 h). Note that the peak number of proximal axonal swellings moves from P2 to P3 and then to 4 from 12 h to 24 h to 48 h post-TBI, respectively. The peak number of distal axonal swellings also shows significant redistribution from D2 to D3, to D4 from 12 h to 24 h, to 48 h post-TBI, respectively. This is consistent with progressive axonal dieback both proximally and distally over time post-TBI. The bar graph (**B**) shows in more detail the statistical difference at each location. Specifically, in those segments 200 $\mu$m–600 $\mu$m proximal to the initial focus of injury (P2 and P3), the number of axonal swellings at 12 h post-TBI is significantly higher than those of 24 h and 48 h post-TBI. These confirm the qualitative impression of the regression of proximal axonal swellings. In contrast, at 600 $\mu$m–1200 $\mu$m distal to the initial focus of injury (D4, D5, and D6), the number of axonal swellings at 24 h post-TBI is higher than that of 12 h post-TBI, while at 48 h post-TBI the number is again significantly higher than those of 12 h and 24 h post-TBI. These confirm the qualitative impression of the retention of distal axonal swellings (*$p < 0.05$, **$p < 0.01$, ***$p < 0.001$).

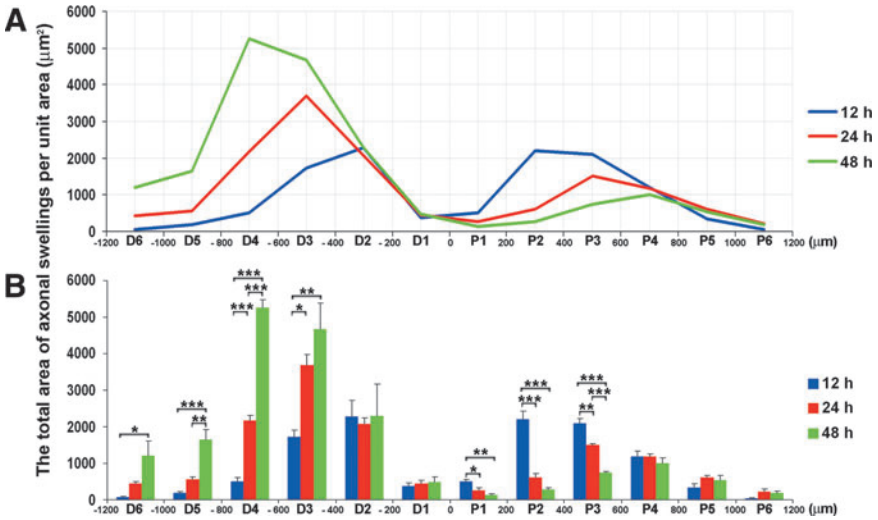


**FIG. 8.** A plot of the total area of axonal swellings per unit area and their distribution along the optic nerve over time. Here again we display both in line (**A**) and bar (**B**) graph formats the total area of axonal swellings per unit area, which equals the sum of the area of each swelling in each individual grid. The line graph (**A**) best illustrates the change of the total axonal swelling area and its distribution along the optic nerve over time (blue = 12 h, red = 24 h, and green = 48 h). Note that the peak of the total area of proximal axonal swellings moves from P2 at 12 h, to P3 at 24 h, and further to P4 at 48 h post-TBI. The peak of total area of distal axonal swellings shows significant redistribution from D2 at 12 h, to D3 at 24 h, and further to D4 at 48 h post-TBI. This again demonstrates progressive axonal dieback both proximally and distally post-TBI. The bar graph (**B**) reveals in more detail the statistical deference at each individual location. Specifically, in those segments 200 $\mu$m–600 $\mu$m proximal to the initial focus of injury (P2 and P3), the total area of axonal swellings at 12 h post-TBI is significantly higher than those of 24 h and 48 h post-TBI. These confirm the qualitative impression of the regression of proximal axonal swellings. In contrast, at 400 $\mu$m–800 $\mu$m distal to the initial focus of injury (D3 and D4), the total area of axonal swellings at 24 h post-TBI is higher than that of 12 h post-TBI. At 400 $\mu$m–1200 $\mu$m distal to the initial focus of injury (D3, D4, D5, and D6), the total area of axonal swellings at 48 h post-TBI is higher than that of 12 h post-TBI. These again suggest the retention of distal axonal swellings over time (*$p < 0.05$, **$p < 0.01$, ***$p < 0.001$).

area did not reveal robust significant changes over time along the length of the optic nerve (data not shown).

### *Relationship between the above-described YFP-linked changes and established markers of TAI (APP)*

To compare the above results of progressive proximal and distal axonal swellings obtained from the YFP-16 transgenic mice to the previous data gained from the use of biological markers of axonal pathology, including those targeting APP, a dual fluorescence approach was employed. At all time points post-TBI, the use of antibodies to APP alone revealed immunoreactive axonal swellings consistent with previous descriptions (Fig. 9). However, when these same nerve segments were examined via confocal microscopy to visualize both the endogenous YFP as well as the antibodies to the C-terminus of APP, an unanticipated response was seen. Specifically, in this approach, we noted that the antibodies to the C-terminus of APP mapped exclusively to proximal swellings, with no evidence of distal immunoreactivity, despite the presence of numerous large and well-formed distal YFP-positive swellings (Fig. 9).

### *Evidence for blood–brain barrier disruption and the retention of axons in the region of YFP fluorescence quenching*

As noted previously, the delayed regional loss of YFP fluorescence observed in the current study was potentially related to fluorescence quenching and not to the over-loss of fiber coursing through this region. To assess this potential and its impact upon our data analysis, we probed the injured YFP optic nerve sections with antibodies to assess the BBB integrity (antibodies to endogenous IgG), as well as antibodies targeting the retention of potentially YFP fluorescence-quenched axons (the antibody to GFP recognizes the endogenous YFP; Sprecher and Desplan, 2008). As early as 1 h post-TBI, Texas-Red fluorescent IgG mapped to the region of YFP fluorescent loss in the damaged optic nerve (Fig. 10A, B, and C), with the caveat that this IgG penetrance was not seen in control animals. The zone of IgG Texas-Red fluorescence expanded further at 3 h post-TBI (Fig. 10D, E, and F), and again mapped to the now expanded locus of YFP fluorescence loss. This extravasation of IgG was interpreted to reflect a focal perturbation of the BBB, with the passage of serum proteins into the interstitial space. Further, it was assumed that this protein passage most likely involved the concomitant movement of water, with the formation of edema, all of which were also consistent with our EM observations of edematous-like change occurring in the expanding interstitium (Fig. 3). It is important to note that this barrier disruption, associated with IgG passage into the optic nerve, was not linked to the presence of either overt or petechial hemorrhage, suggesting a more subtle form of BBB perturbation.

Despite the breakdown of the BBB and the loss of YFP fluorescence, we also observed the persistence of intact/unaltered axons, as well as detached and fragmented axons, in these same regions via the use of antibodies targeting endogenous YFP. Specifically, as shown in Figure 11, through the anti-GFP antibody's positive immunoreactive staining of

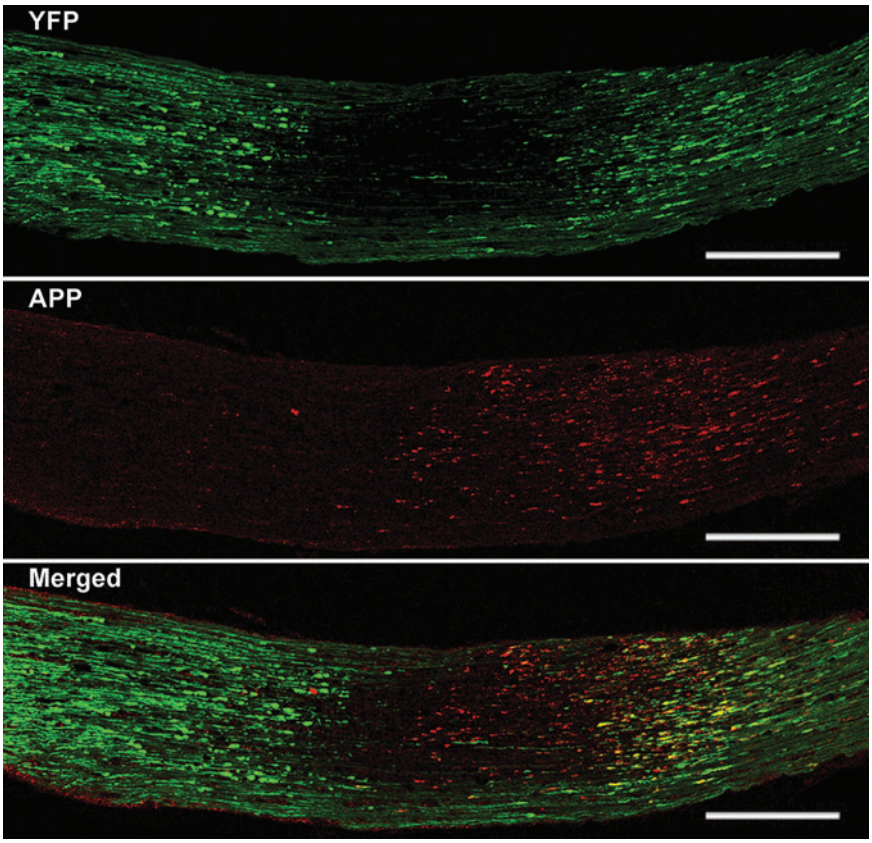


**FIG. 9.** The relationship between the YFP-linked axonal changes and the APP immunofluorescence staining via confocal microscopy. As noted above, axonal swellings can be readily visualized by their YFP fluorescence at both the proximal and the distal optic nerve segments at 12 h post-TBI. Note that at this time point the APP immunoreactivity is found exclusively in the proximal segments, whereas it co-localizes with the YFP fluorescence (yellow in the merged image). In contrast, in the distal segment, there is no APP immunoreactivity despite the presence of numerous YFP-positive axonal swellings. Here the chiasm is to the left and the globe is to the right (scale bar = 200 $\mu$m).

the endogenous YFP, the optic nerve at 24 h post-TBI revealed the existence of unaltered axons coursing through the locus of fluorescence quenching, together with scattered damaged axonal profiles again consistent with TAI.

## Discussion

This study illustrates that a model of traumatic brain injury is capable of evoking traumatic axonal change within the optic nerve that can be evaluated in a consistent fashion. The current study's use of YFP-expressing mice provides an unprecedented view into the pathogenesis of traumatic induced axonal injury, allowing for the precise identification of the initiation of axonal injury and the subsequent progression of axonal swelling and disconnection, as well as the ongoing proximal and distal axonal response. To date, others have studied traumatic axonal injury using optic nerve stretch (Maxwell and Graham, 1997; Maxwell et al., 1990; Saatman

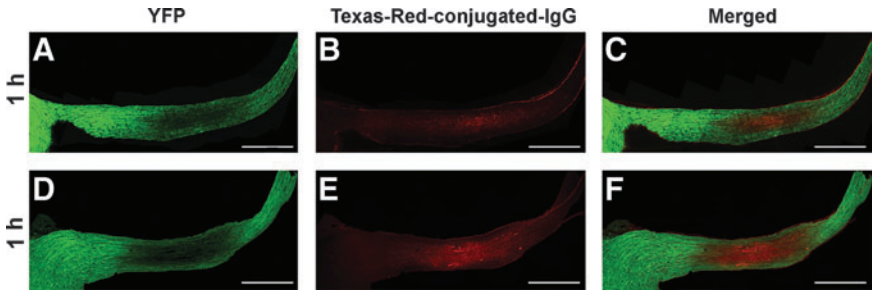


**FIG. 10.** Texas-Red-conjugated IgG maps to the region of YFP fluorescence quenching in the optic nerve of Thy1-YFP-16 mice. Note that at 1 h post-TBI, the region of fluorescent loss (**A**) directly correlates with the IgG immunoreactivity (**B** and **C**). Further, note that the locus of YFP fluorescent loss is expanded at 3 h post-TBI (**D**), which also corresponds to the Texas-Red-conjugated IgG localization (**E** and **F**; scale bar = 500 $\mu$m; YFP, yellow fluorescent protein; TBI, traumatic brain injury).

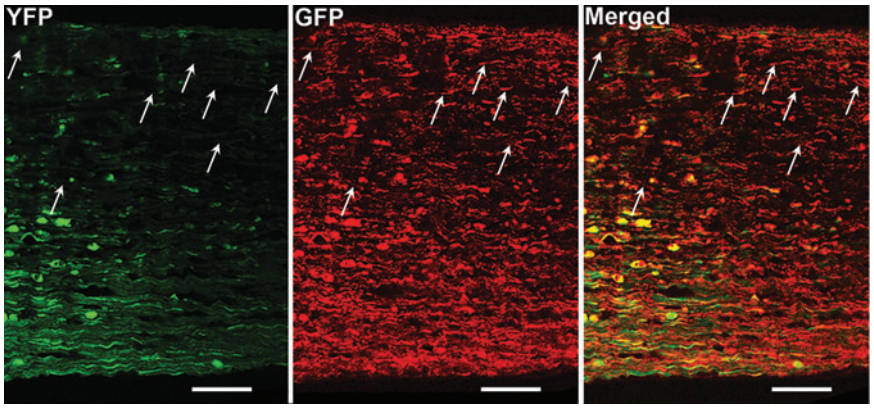


**FIG. 11.** The retention of YFP-expressing axons in the region of fluorescence quenching. With confocal microscopy, at 24 h post-TBI, the YFP fluorescently-quenched axons can now be visualized by antibodies targeting GFP (arrows) in a distal optic nerve segment. This suggests that despite axonal YFP fluorescence quenching, intact axons are retained in the same field (scale bar = 50 $\mu$m).

et al., 2003; Serbest et al., 2007; Sulaiman et al., 2010), and these studies have provided important information on the progressive changes associated with traumatically-induced axonal injury. While one could argue that the reactive changes seen within the optic nerve following cFPI mirror those observed with the optic nerve stretch model, differences do exist. Although both injury models involve predominantly the prechiasmatic region, cFPI, in contrast to optic nerve stretch (Gennarelli, et al., 1989), involves less prominent axonal damage over the length of the optic nerve. Further, following cFPI, blood–brain barrier disruption is seen within the optic nerve. This appears consistent with the brain parenchymal barrier disruption seen following fluid-percussion brain injury that has been linked to concomitant brain deformation and compression (Povlishock et al., 1978). Such differences between the optic nerve injury induced by cFPI versus optic nerve stretch suggest that unlike optic nerve stretch models, cFPI involves a stretch as well as a compression/deformation component that participates in the subsequent pathological response. Irrespective of the causative factors and their specific relationship to the pathobiology of TBI, the current animal model offers another important characteristic that further distinguishes it from the optic nerve stretch model. Specifically, unlike optic nerve stretch, cFPI also evokes TAI throughout the related brain parenchyma, which is entirely consistent with our recent finding of TAI within the neocortex, hippocampus, and thalamus of comparably injured YFP-H mice (Greer et al., 2011). This is of more than academic interest in that we envision that the currently described optic nerve injury model via its routine quantitative assessment of axonal damage will allow for rapid preclinical therapeutic screening using either IV, IP, or intrathecal routes of therapy administration. The perceived benefit of this current cFPI-induced optic nerve injury model resides in the fact that if any therapy is judged to be protective within the optic nerve, such protection could then be easily screened in the brain parenchyma of these same animals, thereby providing more compelling evidence of generalized therapeutic efficacy.

In the current investigation using a model of brain and optic nerve injury, we demonstrated within the optic nerve, the involvement of multiple axons typically found in relation to other unaltered axons. Consistent with previous descriptions of the pathogenesis of TAI, our studies confirmed that this optic nerve involvement did not involve physical transection of the axon or the concomitant involvement of local destructive vascular lesions (Maxwell et al., 1997; Povlishock et al., 1983; Povlishock and Kontos, 1985). Rather, the injury evoked in YFP-expressing axons was scattered swellings that underwent lobulation, leading to disconnection over a 1- to 3-h post-TBI period. Particularly significant in the current communication was the parallel finding of the relatively rapid dieback of both the proximal and distal disconnected segments, together with the rapid regression of the proximal swollen axonal segment, and the persistence of the degenerating distal swelling. To our knowledge, these findings have not been previously described in either the experimental TBI animal or human forensic literature. As seen in the data provided, relatively significant dieback occurred in both the proximal and distal segments within 48 h following injury, wherein the injured segments moved approximately 0.4–0.8 mm in both the proximal and distal directions. While such dieback has not been previously described in the context of TBI, spatially and temporally similar dieback has been described following spinal cord injury (Horn et al., 2008; Kerschensteiner et al., 2005; Oudega et al., 1999), and laser-induced *in vitro* axonal damage (Hellman et al., 2010). With spinal cord injury such dieback has been linked to macrophage infiltration and possible substrate modification (Busch et al., 2009; Horn et al., 2008), while *in vitro* studies suggest that calcium dysregulation plays an important role (Hellman et al., 2010). Given the differences between TBI and *in vivo* spinal cord injury and *in vitro* laser injury, the actual mechanisms involved in this dieback remain unclear, and perhaps may involve a combination of all the above factors. In relation to this process of axonal dieback, it is also of note that the singular distal swellings observed in the current study are at variance with the wallerian changes described following physical transection of the optic nerve, wherein wallerian degeneration was associated with relatively dramatic axonal beading along the continuous axonal segment distal to the transection (Beirowski et al., 2010). This difference is most likely consistent with the nature of TAI, which does not evoke the dramatic local destructive change typically associated with the studies of wallerian degeneration evoked by optic

nerve transection (Beirowski et al., 2010), and/or the fiber damage seen with optic nerve ligation or crush (Knöferle et al., 2010). Although it is difficult to directly extrapolate from a static image the actual progression of a dynamic process, our parallel EM analysis proved useful in assessing the fate of the proximal and distal swellings. As noted, the distal swellings routinely demonstrated increased electron density, together with significant mitochondrial disruption, all of which are consistent with their degeneration and subsequent dieback.

In concert with the above observations focusing on the distal swellings, our evaluation of the proximal axonal swellings also provided significant, previously unreported insight into the progression of TAI. Our quantitative and qualitative studies confirmed the dieback of the proximal axonal swellings that moved proximally over time. As noted, such injured axons were seen adjacent to other intact fibers, although this relationship was somewhat obscured by the presence of local tissue edema and fluorescence quenching, an issue which will be discussed below. While the proximal segment, like its distal stump, revealed dramatic dieback, it also manifested a previously unappreciated response in which it underwent a relatively rapid transition from an enlarged and swollen to a thinned and truncated appendage. Parallel ultrastructural studies substantiated this finding and suggested that the dieback of the axonal swelling and its formation of the truncated appendage were not related to overt degeneration, but rather some form of axonal reorganization. In fact, this dynamic reorganization appeared consistent with the conversion of anterograde to retrograde axonal transport, which has been suggested in other experimental studies (Martz et al., 1989; Sahenk and Lasek, 1988).

In concert with the above observations, another unanticipated finding centered on the observation that antibodies targeting C-terminus APP mapped exclusively to the proximal axonal segments, with virtually no evidence of distal swelling immunoreactivity at all the delayed time points assessed. Antibodies to APP have been widely used in animal studies and human forensic analysis (Hortobagyi et al., 2007; Sherriff et al., 1994a, 1994b; Stone et al., 2000), yet there has been no widespread appreciation of what component of the injured axon is delineated by APP. Further complicating this issue is also the fact that there has been no consideration of the potential that different antibodies targeting different APP epitopes may yield different responses. Our antibodies which target APP's C-terminus consistently mapped to the proximal swelling, without targeting to the distal swelling. In contrast, in studies of wallerian degeneration within the optic nerve, using antibodies targeting the N-terminus of APP, Beirowski and colleagues (2010) demonstrated APP targeting of the distal swelling, although in these studies there was no attempt to evaluate the immunoreactivity of the proximal axonal segment. The difference between our study and that of Beirowski and colleagues most likely reflects epitope specificity, with the caveat that the degenerative change ongoing in the distal degenerating segment may undergo proteolytic cleavage of the C-terminus with the exposure of the N-terminus, an issue which will obviously require further evaluation. This observation also takes on increased importance in the context of human forensic studies, wherein the use of antibodies to the N-terminus is the norm, raising the issue as to whether the use of such antibodies may lead to either an over- or underappreciation of the overall burden of axonal injury both in studies of adult brain injury and child abuse.

Although we have emphasized the scattered nature of axonal change occurring within the optic nerve, we have also observed that this phenomenon was negatively influenced by the presence of local CNS BBB disruption and edema, which correlated with local quenching of the endogenous YFP fluorescence. Such non-hemorrhagic BBB disruption is a well-recognized feature of mild TBI, and our lab has previously identified comparable barrier disruption and protein extravasation within the brainstem and neocortex following TBI (Kelley et al., 2007; Povlishock et al., 1978). The linkage of BBB disruption to fluorescent quenching is supported by the observation that all zones of local fluorescence loss mapped precisely to concomitant alterations in BBB status, as assessed by the passage of the endogenous immunoglobulin IgG. The suggestion here is that the parallel movement of water with the IgG participated in the fluorescent quenching. While this phenomenon has not been described in the context of fluorescently-expressing transgenic animals, it has been demonstrated that water and solvent properties of water can result in fluorescence quenching by multiple mechanisms such as hydrogen-bond interactions (Oshima et al., 2006), photoionization (Sadkowski and Fleming, 1980), the transition to a close-lying energy level (Tobita et al., 2001), intersystem crossing (Seliskar and Brand, 1971), and specific solute–solvent interactions (Ebbesen and Ghiron, 1989). Since optic nerve edema most likely involves significant water generation (Donkin and Vink, 2010), it is not unreasonable to assume that this water can participate in fluorescence quenching via either one or several of the above-described mechanisms. The correctness of this assumption is further supported by our parallel investigations using antibodies to the endogenous YFP, which consistently labeled fibers independent of their YFP fluorescence, via our reliance on a chromogen-based approach. This strategy confirmed that the loss of fluorescence was most likely due to quenching, and not associated with actual fiber loss.

In summary, this study reveals TBI-induced TAI within the optic nerve. Further, these observations within the optic nerve provide unique insight into the pathobiology associated with TAI, particularly in terms of axonal swelling, disconnection, and proximal and distal dieback changes not well appreciated in the highly complex brain environment. We also demonstrate that this optic nerve approach provides via its regional specificity, the opportunity for rigorous quantification. This provides the potential for multiple future applications utilizing the rigorous assessment to evaluate various therapeutic interventions in attenuating axonal damage, while also permitting the evaluation of anterograde downstream neuronal and/or synaptic plasticity, and/or the assessment of retrograde upstream neuronal injury.

## Acknowledgments

This research is supported by grants HD055813 and 5P30NS047463. We thank Raymond Colello, Scott Henderson, Susan A. Walker, Lynn Carol Davis, Sharon Toussaint, and Jesse A. Sims for their technical assistance and guidance in various aspects of this study.

## Author Disclosure Statement

No competing financial interests exist.

## References


Beirowski, B., Nogradi, A., Babetto, E., Garcia-Alias, G., and Coleman, M.P. (2010). Mechanisms of axonal spheroid formation in central nervous system Wallerian degeneration. J. Neuropathol. Exp. Neurol. 69, 455–472.

Belanger, H.G., Vanderploeg, R.D., Curtiss, G., and Warden, D.L. (2007). Recent neuroimaging techniques in mild traumatic brain injury. J. Neuropsychiatry Clin. Neurosci. 19, 5–20.

Blumbergs, P.C., Jones, N.R., and North, J.B. (1989). Diffuse axonal injury in head trauma. J. Neurol. Neurosurg. Psychiatry 52, 838–841.

Blumbergs, P.C., Scott, G., Manavis, J., Wainwright, H., Simpson, D.A., and McLean, A.J. (1995). Topography of axonal injury as defined by amyloid precursor protein and the sector scoring method in mild and severe closed head injury. J. Neurotrauma 12, 565–572.

Büki, A., Farkas, O., Doczi, T., and Povlishock, J.T. (2003). Preinjury administration of the calpain inhibitor MDL-28170 attenuates traumatically induced axonal injury. J. Neurotrauma 20, 261–268.

Büki, A., Okonkwo, D.O., Wang, K.K., and Povlishock, J.T. (2000). Cytochrome c release and caspase activation in traumatic axonal injury. J. Neurosci. 20, 2825–2834.

Busch, S.A., Horn, K.P., Silver, D.J., and Silver, J. (2009). Overcoming macrophage-mediated axonal dieback following CNS injury. J. Neurosci. 29, 9967–9976.

Christman, C.W., Grady, M.S., Walker, S.A., Holloway, K.L., and Povlishock, J.T. (1994). Ultrastructural studies of diffuse axonal injury in humans. J. Neurotrauma 11, 173–186.

Deng-Bryant, Y., Singh, I.N., Carrico, K.M., and Hall, E.D. (2008). Neuroprotective effects of tempol, a catalytic scavenger of peroxynitrite-derived free radicals, in a mouse traumatic brain injury model. J. Cereb. Blood Flow Metab. 28, 1114–1126.

Dixon, C.E., Lyeth, B.G., Povlishock, J.T., Findling, R.L., Hamm, R.J., Marmarou, A., Young, H.F., and Hayes, R.L. (1987). A fluid percussion model of experimental brain injury in the rat. J. Neurosurg. 67, 110–119.

Donkin, J.J., and Vink, R. (2010). Mechanisms of cerebral edema in traumatic brain injury: therapeutic developments. Curr. Opin. Neurol. 23, 293–299.

Ebbesen, T.W., and Ghiron, C.A. (1989). Role of specific solvation in the fluorescence sensitivity of 1,8-ANS to water. J. Phys. Chem. 93, 7139–7143.

Farkas, O., and Povlishock, J.T. (2007). Cellular and subcellular change evoked by diffuse traumatic brain injury: A complex web of change extending far beyond focal damage. Prog. Brain Res. 161, 43–59.

Feng, G., Mellor, R.H., Bernstein, M., Keller-Peck, C., Nguyen, Q.T., Wallace, M., Nerbonne, J.M., Lichtman, J.W., and Sanes, J.R. (2000). Imaging neuronal subsets in transgenic mice expressing multiple spectral variants of GFP. Neuron 28, 41–51.

Gao, G., Oda, Y., Wei, E.P., and Povlishock, J.T. (2010). The adverse pial arteriolar and axonal consequences of traumatic brain injury complicated by hypoxia and their therapeutic modulation with hypothermia in rat. J. Cereb. Blood Flow Metab. 30, 628–637.

Gennarelli, T.A., Thibault, L.E., Tipperman, R., Tomei, G., Sergot, R., Brown, M., Maxwell, W.L., Graham, D I., Adams, J.H., and Irvine, A. (1989). Axonal injury in the optic nerve: a model simulating diffuse axonal injury in the brain. J. Neurosurg. 71, 244–253.

Gleckman, A.M., Bell, M.D., Evans, R.J., and Smith, T.W. (1999). Diffuse axonal injury in infants with nonaccidental craniocerebral trauma: Enhanced detection by beta-amyloid precursor protein immunohistochemical staining. Arch. Pathol. Lab. Med. 123, 146–151.

Graham, D.I., Gennarelli, T.A., and McIntosh, T.K. (2002). Trauma, in: *Greenfield*'s *Neuropathology*. D.I. Graham, and P.L. Lantos, (eds). London: Arnold Publishers. pps. 823–898.

Greer, J.E., McGinn, M.J., and Povlishock, J.T. (2011). Diffuse traumatic axonal injury in the mouse induces atrophy, c-Jun activation, and axonal outgrowth in the axotomized neuronal population. J. Neurosci. 31, 5089–5105.

Hall, E.D., Vaishnav, R.A., and Mustafa, A.G. (2010). Antioxidant therapies for traumatic brain injury. Neurotherapeutics 7, 51–61.

Hellman, A.N., Vahidi, B., Kim, H.J., Mismar, W., Steward, O., Jeon, N.L., and Venugopalan, V. (2010). Examination of axonal injury and regeneration in micropatterned neuronal culture using pulsed laser microbeam dissection. Lab. Chip. 10, 2083–2092.

Horn, K.P., Busch, S.A., Hawthorne, A.L., van Rooijen, N., and Silver, J. (2008). Another barrier to regeneration in the CNS: activated macrophages induce extensive retraction of dystrophic axons through direct physical interactions. J. Neurosci. 28, 9330–9341.

Hortobagyi, T., Wise, S., Hunt, N., Cary, N., Djurovic, V., Fegan-Earl, A., Shorrock, K., Rouse, D., and Al-Sarraj, S. (2007). Traumatic axonal damage in the brain can be detected using beta-APP immunohistochemistry within 35 min after head injury to human adults. Neuropathol. Appl. Neurobiol. 33, 226–237.

Kelley, B.J., Farkas, O., Lifshitz, J., and Povlishock, J.T. (2006). Traumatic axonal injury in the perisomatic domain triggers ultrarapid secondary axotomy and Wallerian degeneration. Exp. Neurol. 198, 350–360.

Kelley, B.J., Lifshitz, J., and Povlishock, J.T. (2007). Neuroinflammatory responses after experimental diffuse traumatic brain injury. J. Neuropathol. Exp. Neurol. 66, 989–1001.

Kerschensteiner, M., Schwab, M.E., Lichtman, J.W., and Misgeld, T. (2005). In vivo imaging of axonal degeneration and regeneration in the injured spinal cord. Nat. Med. 11, 572–577.

Kilinc, D., Gallo, G., and Barbee, K. (2007). Poloxamer 188 reduces axonal beading following mechanical trauma to cultured neurons. Conf. Proc. IEEE Eng. Med. Biol. Soc. 2007, 5395–5398.

Knöferle, J., Koch, J.C., Ostendorf, T., Michel, U., Planchamp, V., Vutova, P., Tönges, L., Stadelmann, C., Brück, W., Bähr, M., and Lingor, P. (2010). Mechanisms of acute axonal degeneration in the optic nerve in vivo. Proc. Natl. Acad. Sci. USA 107, 6064–6069.

Koizumi, H., and Povlishock, J.T. (1998). Posttraumatic hypothermia in the treatment of axonal damage in an animal model of traumatic axonal injury. J. Neurosurg. 89, 303–309.

Kumar, R., Saksena, S., Husain, M., Srivastava, A., Rathore, R.K., Agarwal, S., and Gupta, R.K. (2010). Serial changes in diffusion tensor imaging metrics of corpus callosum in moderate traumatic brain injury patients and their correlation with neuropsychometric tests: a 2-year follow-up study. J. Head Trauma Rehabil. 25, 31–42.

Marmarou, C.R., and Povlishock, J.T. (2006). Administration of the immunophilin ligand FK506 differentially attenuates neurofilament compaction and impaired axonal transport in injured axons following diffuse traumatic brain injury. Exp. Neurol. 197, 353–362.

Martz, D., Garner, J., and Lasek, R.J. (1989). Protein changes during anterograde-to-retrograde conversion of axonally transported vesicles. Brain Res. 476, 199–203.

Maxwell, W.L., and Graham, D.I. (1997). Loss of axonal microtubules and neurofilaments after stretch-injury to guinea pig optic nerve fibers. J. Neurotrauma 14, 603–614.

Maxwell, W.L., Irvine, A., Strang, R.H., Graham, D.I., Adams, J.H., and Gennarelli, T.A. (1990). Glycogen accumulation in axons after stretch injury. J. Neurocytol. 19, 235–241.

Maxwell, W.L., Povlishock, J.T., and Graham, D.L. (1997). A mechanistic analysis of nondisruptive axonal injury: a review. J. Neurotrauma 14, 419–440.

Maxwell, W.L., Watson, A., Queen, R., Conway, B., Russell, D., Neilson, M., and Graham, D.I. (2005). Slow, medium, or fast re-warming following post-traumatic hypothermia therapy? An ultrastructural perspective. J. Neurotrauma 22, 873–884.

Mbye, L.H., Singh, I.N., Carrico, K.M., Saatman, K.E., and Hall, E.D. (2009). Comparative neuroprotective effects of cyclosporin A and NIM811, a nonimmunosuppressive cyclosporin A analog, following traumatic brain injury. J. Cereb. Blood Flow Metab. 29, 87–97.

Oda, Y., Gao, G., Wei, E.P., and Povlishock, J.T. (2010). Combinational therapy using hypothermia and the immunophilin ligand FK506 to target altered pial arteriolar reactivity, axonal damage, and blood–brain barrier dysfunction after traumatic brain injury in rat. J. Cereb. Blood Flow Metab. Dec. 15. [Epub ahead of print]

Okonkwo, D.O., Büki, A., Siman, R., and Povlishock, J.T. (1999). Cyclosporin A limits calcium-induced axonal damage following traumatic brain injury. Neuroreport 10, 353–358.

Oudega, M., Vargas, C.G., Weber, A.B., Kleitman, N., and Bunge, M.B. (1999). Long-term effects of methylprednisolone following transection of adult rat spinal cord. Eur. J. Neurosci. 11, 2453–2464.

Oshima, J., Yoshihara, T., and Tobita, S. (2006). Water-induced fluorescence quenching of mono- and dicyanoanilines. Chem. Physics Lett. 423, 306–311.

Pettus, E.H., and Povlishock, J.T. (1996). Characterization of a distinct set of intra-axonal ultrastructural changes associated with traumatically induced alteration in axolemmal permeability. Brain Res. 722, 1–11.

Povlishock, J.T., Becker, D.P., Cheng, C.L., and Vaughan, G.W. (1983). Axonal change in minor head injury. J. Neuropathol. Exp. Neurol. 42, 225–242.

Povlishock, J.T., Becker, D.P., Sullivan, H.G., and Miller, J.D. (1978). Vascular permeability alterations to horseradish peroxidase in experimental brain injury. Brain Res. 153, 223–239.

Povlishock, J.T., and Katz, D.I. (2005). Update of neuropathology and neurological recovery after traumatic brain injury. J. Head Trauma Rehabil. 20, 76–94.

Povlishock, J.T., and Kontos, H.A. (1985). Continuing axonal and vascular change following experimental brain trauma. Cent. Nerv. Syst. Trauma 2, 285–298.

Povlishock, J.T. (1992). Traumatically induced axonal injury: pathogenesis and pathobiological implications. Brain Pathol. 2, 1–12.

Reichard, R.R., Smith, C., and Graham, D.I. (2005). The significance of beta-APP immunoreactivity in forensic practice. Neuropathol. Appl. Neurobiol. 31, 304–313.

Saatman, K.E., Abai, B., Grosvenor, A., Vorwerk, C.K., Smith, D.H., and Meaney, D.F. (2003). Traumatic axonal injury results in biphasic calpain activation and retrograde transport impairment in mice. J. Cereb. Blood Flow Metab. 23, 34–42.

Saatman, K.E., Serbest, G., and Burkhardt, M.F. (2009). Axonal damage due to traumatic brain injury, in: *Handbook of Neurochemistry and Molecular Neurobiology: Brain and Spinal Cord Trauma*. N.L. Banik, A. Lajtha, S.K. Ray (eds). New York: Springer, pps. 343–361.

Saatman, K.E., Creed, J., and Raghupathi, R. (2010). Calpain as a therapeutic target in traumatic brain injury. Neurotherapeutics 7, 31–42.

Sadkowski, P.J., and Fleming G.R. (1980). The influence of solvent-solute interaction on radiationless processes: excited state dynamics of anilinonaphthalene sulphonate and related molecules. Chem. Phys. 54, 79–89.

Sahenk, Z., and Lasek, R.J. (1988). Inhibition of proteolysis blocks anterograde-retrograde conversion of axonally transported vesicles. Brain Res. 460, 199–203.

Seliskar, C.J., and Brand, L. (1971). Electronic spectra of 2-aminonaphthalene-6-sulfonate and related molecules. I. General properties and excited-state reactions. J. Am. Chem. Soc. 93, 5405–5414.

Serbest, G., Burkhardt, M.F., Siman, R., Raghupathi, R., and Saatman, K.E. (2007). Temporal profiles of cytoskeletal protein loss following traumatic axonal injury in mice. Neurochem. Res. 32, 2006–2014.

Shagin, D.A., Barsova, E.V., Yanushevich, Y.G., Fradkov, A.F., Lukyanov, K.A., Labas, Y.A., Semenova, T.N., Ugalde, J.A., Meyers, A., Nunez, J.M., Widder, E.A., Lukyanov, S.A., and Matz, M.V. (2004). GFP-like proteins as ubiquitous metazoan superfamily: evolution of functional features and structural complexity. Mol. Biol. Evol. 21, 841–850.

Sherriff, F.E., Bridges, L.R., Gentleman, S.M., Sivaloganathan, S., and Wilson, S. (1994a). Markers of axonal injury in post mortem human brain. Acta Neuropathol. 88, 433–439.

Sherriff, F.E., Bridges, L.R., and Sivaloganathan, S. (1994b). Early detection of axonal injury after human head trauma using immunocytochemistry for beta-amyloid precursor protein. Acta Neuropathol. 87, 55–62.

Sprecher, S.G., and Desplan, C. (2008). Switch of rhodopsin expression in terminally differentiated *Drosophila* sensory neurons. Nature 454, 533–537.

Stone, J.R., Singleton, R.H., and Povlishock, J.T. (2000). Antibodies to the C-terminus of the beta-amyloid precursor protein (APP): A site specific marker for the detection of traumatic axonal injury. Brain Res. 871, 288–302.

Stone, J.R., Walker, S.A., and Povlishock, J.T. (1999). The visualization of a new class of traumatically injured axons through the use of a modified method of microwave antigen retrieval. Acta Neuropathol. 97, 335–345.

Sulaiman, A., Denman, N., Buchanan, S., Porter, N., Vesi, S., Sharpe, R., Graham, D.I., and Maxwell, W. (2010). Stereology and ultrastructure of chronic phase axonal and cell soma pathology in stretch-injured central nerve fibers. J. Neurotrauma [Epub ahead of print].

Tobita, S., Ida, K., and Shiobara, S. (2001). Water-induced fluorescence quenching of aniline and its derivatives in aqueous solution. Res. Chem. Intermed. 27, 205–218.

Wang, J.Y., Bakhadirov, K., Devous, M.D. Sr., Abdi, H., McColl, R., Moore, C., Marquez de la Plata, C.D., Ding, K., Whittemore, A., Babcock, E., Rickbeil, T., Dobervich, J., Kroll, D., Dao, B., Mohindra, N., Madden, C.J., and Diaz-Arrastia, R. (2008). Diffusion tensor tractography of traumatic diffuse axonal injury. Arch. Neurol. 65, 619–626.

Address correspondence to:
*John T. Povlishock, Ph.D.*
*Department of Anatomy and Neurobiology*
*Virginia Commonwealth University Medical Center*
*P.O. Box 980709*
*Richmond, VA 23298*

*E-mail:* jtpovlis@vcu.edu